Response of nanoparticle structure to different types of surface environments: Wide-angle x-ray scattering and molecular dynamics simulations

Hengzhong Zhang,[1,*] Bin Chen,[1] Yang Ren,[2] Glenn A. Waychunas,[3] and Jillian F. Banfield[1,3]
[1]*Department of Earth and Planetary Science, University of California, Berkeley, California 94720, USA*
[2]*Advanced Photon Source, Argonne National Laboratory, Argonne, Illinois 60439, USA*
[3]*Earth Sciences Division, Lawrence Berkeley National Laboratory, Berkeley, California 94720, USA*
(Received 25 August 2009; revised manuscript received 22 February 2010; published 31 March 2010)

The structure of nanoparticles is nonstationary and changes in response to the surface environment where the nanoparticles are situated. Nanoparticle-environment interaction determines the nature of the structure change, an important consideration for evaluating subsequent environmental impact. In this work, we used ZnS nanoparticles to interact with surface environments that contain different inorganic salts, water, and organic molecules. From analysis of the pair-distribution function (PDF) derived from wide-angle x-ray scattering experiments, we found that a stronger surface interaction results in a thicker crystalline core and a thinner distorted shell, corresponding to PDF curves having larger peaks and more peaks at longer radial distances. Plane-wave electronic calculations were used to quantify the interaction strength. An analogous atomic view of the nanoparticle-environmental interactions and structures was provided by molecular dynamics simulations. The extent of response of the nanoparticle structure to various surface environments is used as a measure of the interaction strength between them.

DOI: 10.1103/PhysRevB.81.125444 PACS number(s): 61.46.Df, 61.05.cf, 02.70.Ns

I. INTRODUCTION

When coupled with surface ligands, nanoparticles can be used to target cancer-specific receptors and other malicious cells.[1–3] Functionalized nanoparticles can be used as sensors for detection of deoxyribonucleic acid targets and explosive materials.[4–6] Realization of these nanotechnologies relies on detailed understanding of the nanoparticle structure as well as the interactions between nanoparticles and the surrounding molecules/ions. These interactions include several types of electrostatic interactions (ionic and dipole interactions), covalent bonding, hydrogen bonding, and van der Waals forces. Though atomic force microscopy can measure the forces between nanoparticles and solid surfaces/substrates,[7,8] it is difficult to characterize the details of the interactions between nanoparticles and surface molecules and ions. In particular, the manner in which the nanoparticle structure responds to the surface environments is yet to be explored. In this work, we used atomic pair-distribution function (PDF) analysis to study the structural changes in ZnS nanoparticles due to interactions with different surface species. Molecular simulations were carried out to validate the experimental results and to provide an atomic view of the interaction processes. The approach developed in this work may be used to analyze interaction strengths and effects in nanoparticles that are difficult to measure using other methods. Both the new approach and the acquired knowledge will be advantageous in the development of highly specific nanomaterials for applications in nanomaterial-environment interactions, such as medical/cosmetic products and environmental remediation mechanisms that utilize nanoparticles.[9,10]

II. EXPERIMENTAL

A. Sample preparation

ZnS (sphalerite) nanoparticles with an average diameter of ~3 nm were synthesized in anhydrous methanol. A suspension of 0.09 M ZnS nanoparticles in methanol was prepared by reacting anhydrous zinc chloride ($ZnCl_2$) and sodium sulfide (Na_2S) in anhydrous methanol, followed by purification and redispersion in methanol.[11] For interactions with ZnS nanoparticles, ionic salts (sodium chloride NaCl, calcium chloride $CaCl_2$, and sodium sulfate Na_2SO_4) and molecules having different structures (water H_2O, methanol CH_3OH, thiophenol C_6H_6S, and chlorobenzene C_6H_5Cl) were used as the surface species.

Specific concentrations of different surface species were added to the as-synthesized nano-ZnS suspensions, producing methanol suspensions of 0.07 M ZnS+13.9 M H_2O, 0.06 M ZnS+3.3 M C_6H_5Cl, 0.06 M ZnS+3.3 M C_6H_6S, 0.09 M ZnS+0.03 M NaCl, 0.09 M ZnS +0.015 M $CaCl_2$, and 0.09 M ZnS+0.015 M Na_2SO_4. The new suspensions equilibrated for ~24 h before performing wide-angle x-ray scattering (WAXS) measurements.

B. X-ray diffraction

X-ray diffraction (XRD) was used to identify the phase of the synthesized ZnS and to estimate the crystallite size. XRD specimens were prepared by dispersing a thin layer of the nano-ZnS sample in methanol on to a low-scattering background silicon plate which were then allowed to dry naturally. The plate was loaded immediately into the sample holder of an x-ray diffractometer (PANalytical X'Pert PRO) operated at 40 kV and 40 mA with a Co $K\alpha$ radiation x-ray source (wavelength 1.7903 Å). The XRD pattern was collected at room temperature in the 2θ range of 20°–80° with a scanning rate of 1 °/min.

C. Wide angle x-ray scattering

WAXS measurements were performed at room temperature at the high-energy beamline station 11-ID-C, Advanced

Photon Source, Argonne National Laboratory (USA), with an x-ray wavelength of 0.10770 Å and a sample-to-camera distance of ~272 mm. The exact distance was calibrated using a CeO_2 standard. Small volumes of the ZnS suspensions (containing different concentrations of surface species) were encapsulated in 1.5 mm diameter quartz capillary tubes. These tubes were then put into a capillary tube sample holder for the WAXS experiments. WAXS patterns were acquired at room temperature, with a q (scattering vector) range of 0.3–30 $Å^{-1}$, and a step size of 0.01 $Å^{-1}$. The WAXS signal was captured by an image plate detector. The WAXS patterns of several identical capillary tubes filled with methanol and various surface species (without ZnS nanoparticles) were acquired for background subtraction from the sample patterns.

III. COMPUTATIONAL

A. Electronic structure calculations

To gain insight into the nature of the interactions (such as binding energy, bond length, and electron sharing), we did first-principle calculations of the interactions between one molecular unit of surface species and a bulk ZnS (100) surface. The electronic-structure calculations were carried out using the CPMD package,[12] employing a plane-wave basis (energy cutoff=80 AU) with Troullier-Martins pseudopotentials[13] and a local-density approximation exchange correlation using the high accuracy Padé approximation.[14] A periodic slab of ZnS (~11×11×11 $Å^3$, 32 ZnS molecular units) with a CPMD geometrically optimized (100) surface was used as the basis for interaction with one molecular unit of NaCl, Na_2SO_4, H_2O, C_6H_6S, C_6H_5Cl, and CH_3OH, respectively. Initial setup for a surface species interacting with the ZnS (100) surface for the CPMD electronic calculation was obtained from a classical molecular dynamics (MD) simulation performed using the Forcite module of MATERIALS STUDIO 4.0.[15] In a CPMD geometric optimization, atoms of the interacting surface species were allowed to move in any direction. The coordinates of atoms of the surface species interacting with the ZnS surface were optimized and the energy of the system was minimized using standard criteria [convergence of both orbital (energy and gradient) and geometry to within certain preset variations].[12]

B. Molecular dynamics simulations

In order to correlate the ZnS nanoparticle structure and the strength of the interaction with surface species, we performed MD simulations of three representative systems, nano-ZnS in vacuum (to approximate methanol, see Sec. IV E below), nano-ZnS interacting with water, and nano-ZnS interacting with Na^+/Cl^-. MD simulations of a 3 nm ZnS (sphalerite) particle in vacuum and with adsorption of different numbers of water molecules have been done previously.[16]

MD simulation of adsorption of Na^+/Cl^- ions onto a 3 nm ZnS nanoparticle was performed using the code DL_POLY (Ref. 17) in this work. A shell model with Buckingham-type interatomic potential functions was used to describe the ZnS structure.[18] Using the shell model, a Zn or S atom is treated as a core and a massless (or, very light) shell that are connected by a spring, accounting for ionic polarity induced under a local electric field. The Zn and S atoms have the electrical charges of +2 and −2, respectively. The short-range van der Walls interaction between two atoms i and j takes a Buckingham form,

$$u_{ij}(\text{short range}) = A_{ij}\exp\left(-\frac{R_{ij}}{\rho_{ij}}\right) - \frac{C_{ij}}{R_{ij}^6}, \quad (1)$$

where u_{ij} is the interaction potential, R_{ij} the distance between atoms i and j, and A_{ij}, ρ_{ij}, and C_{ij} are three model parameters. An angle-bending form of three-body interactions is considered for nearest S-Zn-S atoms,

$$u_{ijk} = \frac{1}{2}k_{ijk}(\theta - \theta_{ijk})^2, \quad (2)$$

where u_{ijk} is the interaction potential, k_{ijk} a model parameter, θ the angle formed by atoms i (S), j (Zn, center) and k (S), and θ_{ijk} the equilibrium value of the angle (109.4°).

The interatomic interactions in NaCl were described by the Born-Huggins-Mayer potential functions, which has the same form as Eq. (1) but with an additional term of $-D_{ij}/(R_{ij})^8$ (D_{ij} is a model parameter).[19] For detailed values of the model parameters for ZnS and NaCl, the readers are referred to Refs. 18 and 19. Suitable potential functions for the interaction between ZnS and NaCl are not available from the literature. Thus, we developed interatomic potential functions for the NaCl-ZnS system as described below (Sec. IV D).

In the MD simulation, 24 Na^+/Cl^- ions (to simulate the low concentration of NaCl due to the low solubility in methanol in the experiment) were placed over the surface (with a initial distance of ~3 Å between them) of a 3 nm ZnS nanoparticle constructed from the bulk structure of sphalerite. The MD simulation was carried out at 300 K for a MD time of 20 ps with a step of 10^{-5} ps first and then for another 60 ps with a step of 10^{-4} ps. Potential-energy evolution showed that after ~45 ps, the system has converged to a steady state.

IV. RESULTS AND DISCUSSION

A. Sample characterization

Inspection of the XRD pattern (Fig. 1) shows that the as-synthesized ZnS is nanosphalerite with very broad diffraction peaks. The XRD line profile was analyzed using a numerical method[20] for separation of the overlapping sphalerite (111), (200), (220), and (311) peaks which show significant broadening at the nanoscale size. The Scherrer size[21] of the nano-ZnS was estimated to be ~1.5 nm in diameter using the full width at the half maximum of the (111) peak (with a Scherrer constant of 0.90). This size corresponds to the crystalline core of the ZnS nanoparticles while the physical diameter determined by transmission electron microscopy and UV-vis spectroscopy was ~3 nm.[11] These values show that the as-synthesized ZnS nanoparticles are highly distorted core-shell structures with a weakly diffracting surface layer ~0.75 nm in thickness.

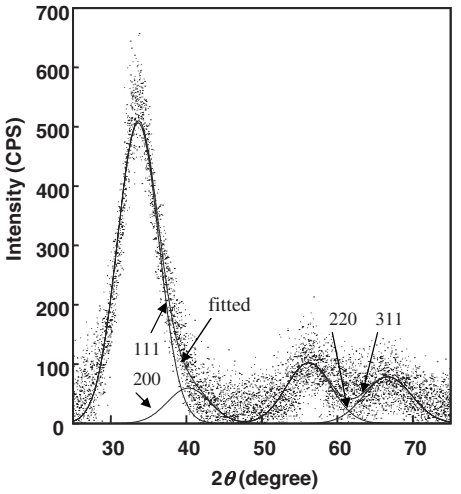

FIG. 1. XRD pattern (dots) of nano-ZnS synthesized in methanol. Overlapping sphalerite (111), (200), (220), and (311) peaks were separated (lines) using a numerical decomposition method (Ref. 20) for estimation of the crystalline core size.

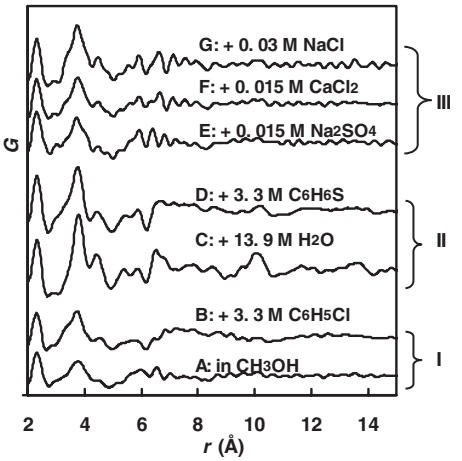

FIG. 2. Atomic pair-distribution function (G) of ~3 nm ZnS nanoparticles (0.06–0.09 M ZnS) suspended in methanol (A) and methanol plus various surface species (B–G). Group I represents surface species with weak interactions with nanoparticles, group II with enhanced interactions, and group III with strong interactions.

B. PDF analysis

PDF analysis has been used to study structures of nanomaterials, including metals (e.g., nano-Au), semiconductors (e.g., nano-CdSe), metal sulfides (e.g., nano-MoS_2), and metal oxides (e.g., nano-TiO_2), as reviewed in Refs. 22–24. However, systematic study of environmental response of nanoparticle structure using PDF analysis was not reported previously.

In this work, the PDFs of ZnS nanoparticles upon interaction with various surface species were derived from the WAXS data. First, structure factors of the nanoparticles were derived from the WAXS patterns after data reduction.[25] Then, the PDFs, or $G(r)$ functions, were obtained through Fourier transform of the structure factors $S(q)$,[25]

$$G(r) = \frac{2}{\pi}\int_0^\infty q[S(q)-1]\sin(qr)dq. \quad (3)$$

PDF patterns reflect the atomic correlations in a material. The theoretical PDF of a bulk crystalline material consists of a series of peaks extending to arbitrarily large radial distance. Experimental PDF peaks are damped with increasing radial distance because of limited experimental resolution (for beamline 11-ID-C at APS, this is at a radial distance of ~7 nm) or because the particles themselves have dimensions smaller than the resolution limit. For our ZnS nanoparticles interacting with various surface ligands, we observed enhanced damping at radial distances smaller than the nanoparticle diameter (Fig. 2), which indicates that the outer parts of the nanoparticles have less-crystalline character than the cores. This must be due to structural distortion of the tetrahedral coordination of Zn or S atoms near the surface.[11,26] As there is a correspondence between different ligand type and the degree of PDF damping, we theorize that the structural distortion (Fig. 2) is specific to the surface ligand and hence the nanoparticle environment. We now quantify how the ligand-surface interaction induces this structural disorder.

The PDF curves in Fig. 2 can be classified into three groups. In group I, there are PDF patterns characterized by a few small peaks at $r < \sim 8$ Å. The relative magnitude of the second broad peak ($r \sim 3.74-3.77$ Å) is lower than or comparable to that of the first peak ($r \sim 2.33$ Å, the average Zn-S bond length). This is the case for nano-ZnS in methanol and methanol+chlorobenzene. In group II, the PDF peaks are larger and more numerous than in group one (r extends to ~14 Å). The relative magnitude of the second broad peak ($r \sim 3.76-3.80$ Å) is higher than that of the first peak ($r \sim 2.33$ Å). In this category are patterns from nano-ZnS in methanol+water and methanol+thiophenol. In group III, the PDF patterns contain many medium to large PDF peaks at $r < \sim 10$ Å (beyond which the minor peaks are noises from data reduction). This group includes nano-ZnS in methanol +dilute inorganic salts (NaCl, $CaCl_2$, and Na_2SO_4). The relative magnitude of the second broad peak ($r \sim 3.72-3.76$ Å) varied from almost comparable to higher than that of the first peak ($r \sim 2.33$ Å). Compared to group I, the peaks in ~5.5–7.5 Å are more significant in this group even though the salt concentrations are much lower than those of methanol and chlorobenzene in group I.

The unequal structural responses (as shown by the PDF curves in Fig. 2) of the ZnS nanoparticles to different surface species are expected to be determined by the interaction strength between the nanoparticles and the surface species. Results from the plane-wave electronic structure calculations (below) are used to determine the binding strength of the surface species and to correlate these with the different induced PDF characters.

C. Nature of surface binding by plane-wave electronic calculations

Table I summarizes results from the electronic-structure calculations. Results show that surface species interact with ZnS (100) surfaces mainly via interactions between their high-electronegativity atoms (O, Cl, and S) and the Zn atoms

TABLE I. First-principle calculated binding energies of surface species interacting with ZnS (100) surface.

Surface species	Major interacting atomic pair[a]	Interatomic distance (Å)	Binding energy (kJ/mol species)
Na_2SO_4	O-Zn	2.083	134.7
NaCl	Cl-Zn	2.332	124.7
C_6H_6S	S-Zn	2.446	89.8
H_2O	O-Zn	2.140	66.7
C_6H_5Cl	Cl-Zn	2.869	78.5
CH_3OH	O-Zn	2.963	36.8

[a]The atomic pair with the shortest distance between the atoms of the surface species and the ZnS (100) surface.

on the ZnS surface (Fig. 3). The equilibrium distance between the interacting atoms is one indication of the strength of the interaction between the surface species and the ZnS surface. A shorter distance usually corresponds to a stronger interaction as the latter usually corresponds to a higher degree of electron sharing and hence a shortening of the internucleus distance. The binding energy represents the energy released when a surface species is adsorbed on the ZnS surface. In general, the higher the binding energy, the greater the structural interaction between the surface species and the ZnS surface.

Table I shows that ionic salts, water and thiophenol, and methanol have binding energies of ~125–135 kJ/mol, 67–90 kJ/mol, and 37 kJ/mol, respectively. These ranges correspond to the different sets of PDF profiles we measured (Fig. 2). For the ionic salts we expect strong binding and thus most surface Zn species is bonded with strengths similar to the underlying Zn-S bonding. A crystal-chemical analysis, e.g., using the Pauling bond valence principle, would hold that these Zn ions are largely valence satisfied. In contrast, for methanol we have weak surface binding, leading to unsatisfied valence contributions on the uppermost Zn ions, which creates structure distortion due to changes in the Zn-S

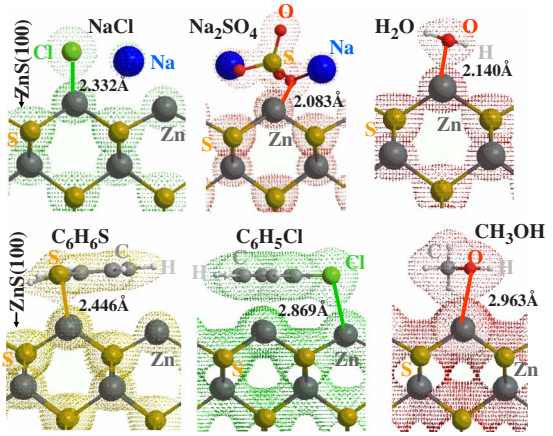

FIG. 3. (Color online) Optimized configurations of surface species interacting with a ZnS (100) surface. Dotted networks are the charge-density isosurfaces of the valence electrons at density values when the isosurfaces of the major interacting atoms (shown in ball-and-stick model) begin to overlap.

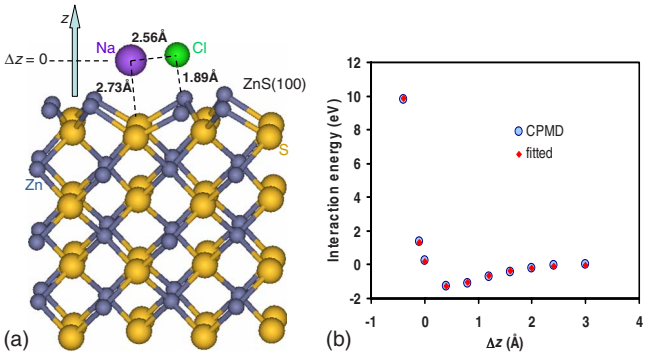

FIG. 4. (Color online) Interaction between a ZnS (100) surface and a NaCl cluster. (a) Structure setup for the calculation of the interaction energy. (b) The interaction energy as a function of the ZnS (100)-NaCl separation. Circles are from CPMD electronic calculations and diamonds from fitting using Morse potential functions [refer Eq. (4) and Table II).

bonding network. For chlorobenzene, though the binding energy is close to those of water and thiophenol, the equilibrium distance between the interacting atoms (Cl-Zn:2.869 Å) is longer than those of the latter two (O-Zn:2.140 Å; S-Zn:2.446 Å). This would decrease the electron sharing between the ZnS surface and chlorobenzene and thus lead to an effect similar to that of methanol on the structure of ZnS. Finally, water and thiophenol represent an intermediate case, with intermediate strength binding, and intermediate size structural distortion. The effects of these strained/distorted surface layers propagate into the nanoparticle interior, causing remarkably distinct PDF characteristics. Molecular dynamics simulations of representative systems provide more details of these structural changes (below).

D. Development of ZnS-NaCl interatomic potential functions

For MD simulation of the interaction between ZnS-NaCl, we developed a set of potential functions by fitting to the interaction energies calculated using the electronic code CPMD (see Sec. III A and Fig. 4). We found that the Morse potential function [Eq. (4)] describes well the pairwise atomic interactions in the ZnS-NaCl system,

$$E(r) = a[\{1 - \exp[-b(r-c)]\}^2 - 1], \tag{4}$$

where E is the interaction energy, r is the interatomic distance, and a, b, and c are adjustable model parameters. Parameter c represents the equilibrium distance between the atoms in a diatomic cluster.

The calculations used the interaction geometry shown in Fig. 4(a). For the NaCl-ZnS interaction, there are four atomic pairs (Na-S, Na-Zn, S-Cl, and Zn-Cl) and hence there are $4 \times 3 = 12$ Morse potential parameters. Simultaneous determination of the 12 parameters could not be achieved from a single fitting of the Morse potential functions to the calculated interaction energies due to the many number of unknown parameters. Thus, as a first step, the three Morse potential parameters (a, b, and c) were derived for an isolated diatomic cluster (Na-S, Na-Zn, S-Cl, or Zn-Cl) by fitting Eq.

TABLE II. Morse potential parameters.

	For diatomic cluster			For ZnS (100)-NaCl cluster		
Atomic pair	*a* (eV)	*b* ($Å^{-1}$)	*c* (Å)	*a* (eV)	*b* ($Å^{-1}$)	*c* (Å)
Na-S	2.0444	1.2145	2.3899	0.4197	1.7098	2.4820
Na-Zn	0.2443	1.2617	2.9917	0.0502	1.7764	3.1071
S-Cl	4.7858	1.4652	2.0511	0.9826	2.0627	2.1301
Zn-Cl	3.8863	1.2503	2.2823	0.7979	1.7602	2.3703

(4) to the interaction energy of the diatomic cluster (calculated using CPMD separately) as a function of the atomic separation. Here, the interaction energy is the energy change by bringing two ions (e.g., Na^+ and Cl^-) from infinitely far away to a designated distance. The obtained parameters are listed in Table II.

We then used the following method to get the Morse potential parameters for the ZnS-NaCl system. As a first approximation, it was assumed that the three parameters (*a*, *b*, and *c*) of the ZnS-NaCl system are proportional to the corresponding ones, respectively, of the diatomic clusters. The proportional coefficients then were optimized such that the differences between the interaction energies calculated from the Morse potential functions and the energies calculated using CPMD became minimal for the ZnS (100)-NaCl cluster system [Fig. 4(b)]. Here, the interaction energy is the energy change by bringing a NaCl cluster to the ZnS (100) surface from infinitely far away to a designated distance. The derived parameters are listed in Table II. One notes that the equilibrium distances *c* are similar in both the diatomic cluster and the ZnS-NaCl system. The derived parameters (Table II) were used for the MD simulation of the interaction between NaCl and a 3 nm ZnS particle.

E. Insight from molecular dynamics simulations

Because the binding energy of methanol on a ZnS surface is low (Table I), the interaction between methanol and ZnS nanoparticles is weak. The weak interaction can be approximated by the MD simulation of a 3 nm ZnS particle in vacuum.[16] The binding energy of water on a ZnS surface is larger than that of methanol (Table I). Hence, the interaction between water and ZnS nanoparticles is stronger and can be studied with MD simulations using sufficient water molecules (e.g., 362 H_2O) to saturate sorption sites on a 3 nm ZnS particle.[16] The MD simulation of the stronger interaction of a 3 nm ZnS particle with 24 Na^+/Cl^- ions was similarly performed in this work (see Sec. III B).

Figure 5 shows (a) snapshots of the MD structures of a 3 nm ZnS particle in vacuum, (b) after adsorption of 362 H_2O molecules, and (c) after adsorption of 24 Na^+/Cl^- ions. Figure 6 shows the comparisons between the PDF curves calculated from the MD structures (Fig. 5) with those from the WAXS determinations (Fig. 2). Results show that the calculated PDF are in good agreement with the experimental PDF. This indicates that the MD simulations can generate atomic structures that are consistent with the WAXS experiments.

Figure 5(a) shows that the 3 nm ZnS nanoparticle in vacuum has a highly distorted shell and a small crystalline core (~1.6 nm in diameter). The core size is close to that (~1.5 nm) estimated from XRD determination for the as-synthesized ZnS nanoparticles in methanol. In contrast, the 3 nm ZnS nanoparticle after adsorption of water molecules [Fig. 5(b)] is more crystalline due to the strong binding of water molecules (energy change due to adsorption of water is

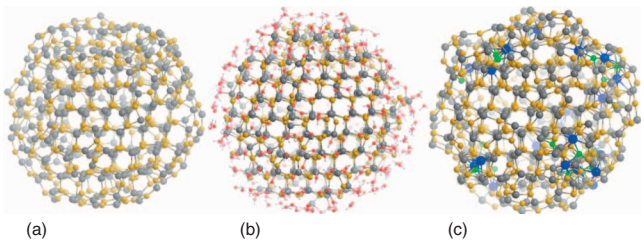

FIG. 5. (Color) Snapshots of the equilibrated structures of a 3 nm ZnS (sphalerite) particle in molecular dynamics simulations. (a) MD in vacuum. (b) MD of nano-ZnS with adsorption of 362 H_2O molecules. (c) MD of nano-ZnS with adsorption of 24 Na^+ and 24 Cl^- ions. Zn: gray; S: dark yellow; O: red; H: light gray; Na: blue; and Cl: green.

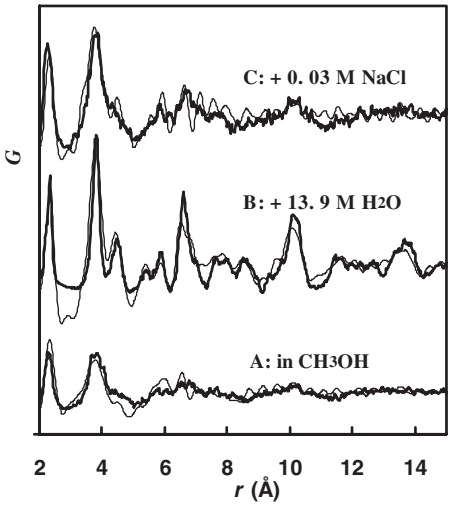

FIG. 6. Comparisons between experimental (thin lines) and calculated PDF (thick lines) of ~3 nm ZnS nanoparticles suspended in methanol (A), methanol plus water (B), and methanol plus NaCl (C). The experimental data are from WAXS determinations and the calculated data are from molecular dynamics simulations.

182 kJ/mol H_2O) and the full coverage of the surface by water molecules. The average Zn-O bond length is 1.988 Å. The 3 nm ZnS nanoparticle after adsorption of 24 Na^+/Cl^- ions [Fig. 5(c)] is also more crystalline than that in vacuum due to the even stronger binding of the ions on the ZnS nanoparticle (energy change due to adsorption of NaCl is 346 kJ/mol NaCl) despite the low number of bound ions. The average Zn-Cl bond length is 2.353 Å and the average Na-S bond length is 2.600 Å.

The MD simulation results show that stronger surface binding and more surface coverage by surface species can largely compensate for the disruption of the periodic structure of the ZnS nanoparticles at the surfaces. This results in a more crystalline nanostructure and hence more well defined and larger R peaks in the PDF.

V. CONCLUSIONS

In this study, we demonstrate that the distortion and core-shell structures of nanoparticles in various chemical environments are determined largely by surface interactions, and that the structural responses to different surroundings can be analyzed by PDFs obtained using high-energy WAXS methods. More and larger PDF peaks at longer radial distances are indicative of stronger surface interactions, as confirmed by first-principle calculations and molecular dynamics simulations. PDF analysis is a sensitive probe of these structural changes, and hence is a general method for the identification and characterization of nanoparticle-surface environment interactions.

ACKNOWLEDGMENTS

We thank B. Gilbert for helpful discussions. Use of the Advanced Photon Source is supported by the U.S. Department of Energy, Office of Science, under Contract No. DE-AC02-06CH11357. Computations were carried out in the Geochemistry Computer Cluster, Lawrence Berkeley National Laboratory. Financial support was provided by the U.S. Department of Energy (Grant No. DE-FG03-01ER15218) and the National Science Foundation (Grant No. EAR-0123967).

*Corresponding author; heng@eps.berkeley.edu

[1] G. J. Kim and S. Nie, Mater. Today **8** (8, Suppl. 1), 28 (2005).
[2] T. M. Fahmy, P. M. Fong, A. Goyal, and W. M. Saltzman, Mater. Today **8** (8, Suppl. 1), 18 (2005).
[3] M. C. Woodle and P. Y. Lu, Mater. Today **8** (8, Suppl. 1), 34 (2005).
[4] N. C. Tansil and Z. Gao, Nanotoday **1** (1), 28 (2006).
[5] F. Patolsky and C. M. Lieber, Mater. Today **8** (4), 20 (2005).
[6] L. Senesac and T. G. Thundat, Mater. Today **11** (3), 28 (2008).
[7] K. L. Chen and S. E. Mylon, Langmuir **23**, 5920 (2007).
[8] Q. K. Ong and I. Sokolov, J. Colloid Interface Sci. **310**, 385 (2007).
[9] A. D. Maynard, Nanotoday **1** (2), 22 (2006).
[10] P. G. Tratnyek and R. L. Johnson, Nanotoday **1** (2), 44 (2006).
[11] H. Zhang, B. Gilbert, F. Huang, and J. F. Banfield, Nature (London) **424**, 1025 (2003).
[12] The CPMD Consortium, CPMD (v3.11) *An ab initio Electronic Structure and Molecular Dynamics Program* (Copyright IBM Corp, 1990–2006; Copyright MPI fuer Festkoerperforschung Stuttgart, 1997–2001).
[13] N. Troullier and J. L. Martins, Phys. Rev. B **43**, 8861 (1991).
[14] S. Goedecker, M. Teter, and J. Hutter, Phys. Rev. B **54**, 1703 (1996).
[15] MATERIALS STUDIO, version 4, Accelrys Inc., San Diego, 2006.
[16] H. Zhang, J. R. Rustad, and J. F. Banfield, J. Phys. Chem. A **111**, 5008 (2007).
[17] W. Smith and T. R. Forster, The DL_POLY v2.13 User Manual, Daresbury Laboratory, Daresbury, Warrington, 2001.
[18] K. Wright and A. Jackson, J. Mater. Chem. **5**, 2037 (1995).
[19] R. Bahadur, L. M. Russell, S. Alavi, S. T. Martin, and P. R. Buseck, J. Chem. Phys. **124**, 154713 (2006).
[20] H. Zhang, B. Chen, B. Gilbert, and J. F. Banfield, J. Mater. Chem. **16**, 249 (2006).
[21] R. Jenkins and R. L. Snyder, *Introduction to X-Ray Powder Diffractometry* (Wiley, New York, 1996).
[22] S. J. L. Billinge and I. Levin, Science **316**, 561 (2007).
[23] S. J. L. Billinge, J. Solid State Chem. **181**, 1695 (2008).
[24] T. Proffen, Rev. Mineral. Geochem. **63**, 255 (2006).
[25] B. Gilbert F. Huang, H. Zhang, G. A. Waychunas, and J. F. Banfield, Science **305**, 651 (2004).
[26] B. Gilbert, F. Huang, Z. Lin, C. Goodell, H. Zhang, and J. F. Banfield, Nano Lett. **6**, 605 (2006).